

Mixed symmetry localized modes and breathers in binary mixtures of Bose-Einstein condensates in optical lattices

H. A. Cruz^{1,2}, V. A. Brazhnyi¹, V. V. Konotop^{1,2,3}, G. L. Alfimov⁴, and M. Salerno⁵

¹*Centro de Física Teórica e Computacional, Universidade de Lisboa, Complexo Interdisciplinar, Avenida Professor Gama Pinto 2, Lisboa 1649-003, Portugal*

²*Departamento de Física, Universidade de Lisboa, Campo Grande, Ed. C8, Piso 6, Lisboa 1749-016, Portugal*

³*Departamento de Matemáticas, E. T. S. Ingenieros Industriales, Universidad de Castilla-La Mancha, 13071 Ciudad Real, Spain*

⁴*Moscow Institute of Electronic Engineering, Zelenograd, Moscow, 124498, Russia*

⁵*Dipartimento di Fisica "E. R. Caianiello", Consorzio Nazionale Interuniversitario per le Scienze Fisiche della Materia (CNISM), Università di Salerno, I-84081, Baronissi (SA), Italy*

We study localized modes in binary mixtures of Bose-Einstein condensates embedded in one-dimensional optical lattices. We report a diversity of asymmetric modes and investigate their dynamics. We concentrate on the cases where one of the components is dominant, i.e. has much larger number of atoms than the other one, and where both components have the numbers of atoms of the same order but different symmetries. In the first case we propose a method of systematic obtaining the modes, considering the "small" component as bifurcating from the continuum spectrum. A generalization of this approach combined with the use of the symmetry of the coupled Gross-Pitaevskii equations allows obtaining breather modes, which are also presented.

PACS numbers: ...

I. INTRODUCTION

Optical lattices are known to be an effective tool for manipulation of matter waves. The induced spatial periodicity allows, in particular, for the existence of various localized structures, not available in homogeneous systems. Such excitations, which are called localized modes (also gap solitons depending on the limit they are considered in) have been intensively studied during the last few years (see e.g. recent reviews [1, 2] and references therein) and observed experimentally in a Bose-Einstein condensate (BEC) of ^{87}Rb atoms [3]. While main attention was devoted to single-component BECs, existence of localized modes was found to be a generic property of multicomponent systems, as well. More specifically, emergence of coupled bright solitons, from the modulational instability of binary mixtures of BECs in optical lattices (OLs), was observed numerically in [4]. In [5], it was shown that OLs can be used to modify the interactions both within and between BEC components, leading to the creation of two-component gap solitons. Existence and stability of 2D and 1D coupled gap solitons in a binary BEC with repulsive interactions was analyzed by means of the variational approximation and numerically in [6]. It was also found that localized modes can exist in atomic-molecular condensates [7], in Bose-Fermi mixtures in OL [8, 9] and in three-component spinor condensates [10].

All the results on binary mixtures of BECs reported so far, concern excitations of the two components characterized by similar scales, i.e. by spatial localization regions, and numbers of particles of the different species having the same order. Also earlier studies were restricted to

modes having density distributions in both components of the same symmetry, whenever the components belong to the same gap (gap solitons belonging to different gaps were addressed in [6]).

In the present paper we report a diversity of novel states observable in two-component BECs embedded in OLs with different symmetry properties of the density distributions with respect to the periodic potential and therefore termed below as *mixed symmetry* modes (or also gap solitons of mixed symmetry). The interaction between the two components of the condensate is crucial for the existence of these modes since they are formed from single component modes which have different stability properties (one stable and the other unstable) in absence of interaction. The interspecies interaction allows for stabilization of the unstable mode in the pair and subsequently for formation of a stable bound state. Mixed symmetry modes exist both for attractive and repulsive inter- and intra-species interactions and represent very stable new excitations of two component BECs in OLs. Stabilization phenomena induced by the interspecies interaction are also possible for equal symmetry states (both symmetric or antisymmetric with respect to a minimum or a maximum of the potential). In this case we find that modes which are both unstable in absence of interaction can form stable equal symmetry bound states in presence of interspecies interaction. Besides stationary states of mixed symmetry we show that non stationary states of mixed symmetry which give rise to breather-like oscillations are also possible. When the inter- and the intra-species interactions are all equal, the two-component breather modes can be constructed from a linear superposition of two mixed symmetry modes

with an unbalanced number of atoms in the two components. On the other hand, we show that breather modes with a balanced numbers of atoms and with a very regular dynamics which persist on a long time scale without any apparent emission of matter, are also possible. Mixed symmetry modes, both of stationary type and of breather type, considerably enlarge the number of stable localized excitations which one can find in BEC mixtures, this showing the richness of these systems with respect to single component BECs.

The paper is organized as follows. In Sec. II we recall the system of coupled Gross-Pitaevskii (GP) equations describing the mixture, specify the parameters to be used for particular numerical simulations, and give a simple physical picture suggesting existence of asymmetric modes. In Sec. III we discuss on particular examples the localized modes of mixed symmetry in the limit ($N_1 \gg N_2$) and study stability of the modes by direct numerical simulations. In Sec. IV we consider large amplitude localized modes both of equal symmetry and of mixed symmetry type. Sec. V is devoted to breathing modes, both with balanced and unbalanced number of atoms, which are obtained by combining the developed approach with the symmetry of the coupled GP equations. In the Conclusion the main outcomes are summarized.

II. STATEMENT OF THE PROBLEM

A. The model

At the zero temperature and a large number of atoms, when quantum fluctuations can be neglected, a diluted binary mixtures of BECs is well described by the coupled GP equations ($j = 1, 2$) [11]

$$i\hbar \frac{\partial \Psi_j}{\partial t} = -\frac{\hbar^2}{2m_j} \Delta \Psi_j + V_j(\mathbf{r}) \Psi_j + \frac{2\pi\hbar^2}{M} \left(\frac{2M}{m_j} a_{jj} |\Psi_j|^2 + a_{j,3-j} |\Psi_{3-j}|^2 \right) \Psi_j. \quad (1)$$

Here m_j is the atomic mass of the j^{th} component, $M = m_1 m_2 / (m_1 + m_2)$ is the reduced mass, and $a_{ij} = a_{ji}$ are the s-wave scattering lengths of the binary interactions. The macroscopic wave functions, Ψ_j , are normalized to numbers of atoms N_j : $\int |\Psi_j|^2 d\mathbf{r} = N_j$, which do not depend on time. The trap potential for the component j , $V_j(\mathbf{r})$, consists of a superposition of a magnetic trap and an OL along the x -direction:

$$V_j(\mathbf{r}) = \frac{m_j \omega_j^2}{2} (\mathbf{r}_\perp^2 + \lambda^2 x^2) + V_0 E_{Rj} U(\kappa x). \quad (2)$$

Here ω_j is the transverse linear oscillator frequency of the component j , λ is the aspect ratio (it is assumed to be equal for both components), d is the lattice constant, $\kappa = \pi/d$, V_0 is the amplitude of OL measured in terms of

the respective recoil energy $E_{Rj} = \hbar^2 \kappa^2 / (2m_j)$, and $U(\cdot)$ is a π -periodic dimensionless function (the lattice profiles are considered to be the same for both components).

We consider cigar-shaped condensates, i.e. the limit $\lambda \ll 1$, at low densities. To specify the scaling we introduce a small parameter of the problem $\epsilon = \kappa a$, where a is an average transverse oscillator length defined as $a = \sqrt{\hbar / (2M\omega)}$, where $\omega = \sqrt{\omega_1 \omega_2}$. Then the applicability of the theory is determined as smallness of a number of particles on the scale of the scattering length, i.e. as $\sqrt{n} |a_{11}| \sim \kappa a = \epsilon \ll 1$, where $n = N\sqrt{\lambda}/a$ is the linear atomic density and $N = N_1 + N_2$ is the total number of atoms. This is the case when the multiple-scale analysis can be applied to reduce (1) to a system of coupled 1D GP equations (see e.g. [1, 4]). By introducing slow dimensionless independent variables $X = \epsilon x/a$ and $T = \epsilon^2 \omega t$ and dimensionless order parameter $\Phi_j = \mathcal{O}(1)$, through the expansion ($j = 1, 2$)

$$\Psi_j = \frac{\kappa}{\sqrt{2|a_{11}|}} \left(\Phi_j + \epsilon \Phi_j^{(1)} + \dots \right) \varphi_j(\mathbf{R}_\perp) e^{-i\omega_j t} \quad (3)$$

with the normalized transverse eigenfunctions

$$\varphi_j(\mathbf{R}_\perp) = \sqrt{\frac{m_j}{2\pi M}} \left(\frac{\omega_j}{\omega_{3-j}} \right)^{\frac{1}{4}} \exp \left(-\frac{m_j}{4M} \sqrt{\frac{\omega_j}{\omega_{3-j}}} \mathbf{R}_\perp^2 \right),$$

we obtain a system of coupled 1D GP equations

$$i \frac{\partial \Phi_j}{\partial T} = -\frac{M}{m_j} \frac{\partial^2 \Phi_j}{\partial X^2} - V_{0j} U(X) \Phi_j + (\chi_j |\Phi_j|^2 + \chi |\Phi_{3-j}|^2) \Phi_j. \quad (4)$$

Here $V_{0j} = V_0 M / m_j$ and the nonlinear coefficients have the following form

$$\chi_j = \sqrt{\frac{\omega_j}{\omega_{3-j}}} \frac{a_{jj}}{|a_{11}|} \quad \text{and} \quad \chi = \frac{(m_1 + m_2) \sqrt{\omega_1 \omega_2}}{(m_1 \omega_1 + m_2 \omega_2)} \frac{a_{12}}{|a_{11}|}.$$

Looking for stationary solutions $\Phi_j \rightarrow \Phi_j e^{-i\mu_j T}$, we obtain the system

$$\mu_j \Phi_j = -\frac{M}{m_j} \frac{d^2 \Phi_j}{dX^2} - V_{0j} U(X) \Phi_j + (\chi_j |\Phi_j|^2 + \chi |\Phi_{3-j}|^2) \Phi_j \quad (5)$$

with μ_1 and μ_2 being the chemical potentials of the first and second components, respectively.

B. The main goal and the terminology

The goal of this paper is to present some families of localized modes and breathers of Eqs. (5) which are typical for multicomponent BECs and which possess interesting symmetry properties. These solutions have been found numerically by means of different methods. The typical difficulty which arise in this problem is to get *a priori*

idea on possible shapes of localized modes which can be used for numerical iterative algorithm. To overcome this difficulty we have used two alternative approaches. The first involves a search of bifurcations for specific solutions of (5) using shooting method (see [12]) as the main tool. The second is the self-consistent approach which has been used before for applications to single-component BECs (see [13]). The self consistent method, indeed, is very convenient for exploring the band structure in presence of nonlinearity and to address to specific modes for which good initial guesses are available. Basically, the shooting method allows one to make a systematic exploration of the whole families of solutions in terms of a single (for single component BECs) parameter (shooting parameter). Similar exploration of the case of coupled GP equations is quite complicated, since in this case one has to scan a semi-infinite domain of two shooting parameters. In the present paper we use the shooting method to investigate localized modes of the mixed symmetry type in the limit $N_1 \gg N_2$ (see Sec. III) and resort to self consistent approach to investigate BEC mixtures with balanced number of atoms (see Sec. IV). When one of the components is dominant, i.e. it has much larger number of atoms than the second component, the last one can be considered as bifurcating from the linear spectrum. Such modes will be referred to as *unbalanced* or strongly asymmetric in number of atoms. In this way after constructing the localized solution for the first component in the absence of the second one, the mode can be constructed by means of some iterative procedure. Combining this approach with the symmetry of the system we will also be able to construct (numerically) exact breathing localized modes.

Another regime we will deal with corresponds to the situation when the both components are large amplitude solutions having numbers of particles of the same order, $N_1 \sim N_2$. In this case we will show existence of not only simplest fundamental modes with equal symmetry but also modes and breathers with mixed symmetry. We remark that mixed symmetry modes were also found in atomic-molecular condensates [7]. In this case, however, the mean-field equations had an intrinsic asymmetry due to the different properties of atoms and molecules.

First of all it is desirable to establish a convenient terminology for the identification of modes. To this end we observe that multiplying (5) by $\partial\Phi_j/\partial X$ and integrating with respect to X one arrives at the *necessary condition* for existence of a stationary localized mode (Φ_1, Φ_2) :

$$\int (V_{01}|\Phi_1|^2 + V_{02}|\Phi_2|^2) \frac{dU(X)}{dX} dX = 0. \quad (6)$$

For the physical interpretation of this condition, we notice that a solution of (5) minimizes the Hamiltonian $H = H_1 + H_2 + H_{12} + H_v(0)$, where

$$H_j = \int \left(\frac{M}{m_j} \left| \frac{\partial\Phi_j}{\partial X} \right|^2 + \frac{\chi_j}{2} |\Phi_j|^4 \right) dX \quad (7)$$

$H_{12} = \chi \int |\Phi_1|^2 |\Phi_2|^2 dX$, and we have defined

$$H_v(\zeta) \equiv \int (V_{01}|\Phi_1|^2 + V_{02}|\Phi_2|^2) U(X - \zeta) dX. \quad (8)$$

Considering $(\Phi_1(X - \zeta), \Phi_2(X - \zeta))$ with $\zeta \ll 1$, which for a stable solution must lead to increase of the energy, we immediately obtain

$$\left. \frac{dH_v(\zeta)}{d\zeta} \right|_{\zeta=0} = 0 \quad \text{and} \quad \left. \frac{d^2 H_v(\zeta)}{d\zeta^2} \right|_{\zeta=0} > 0. \quad (9)$$

The first of the obtained constrains is exactly Eq. (6).

Let us now require the potential to have a definite symmetry, i.e. to be either even or odd, and concentrate on the solutions possessing a specific symmetry, i.e. $\Phi_j(-X) = \pm\Phi_j(X)$. If the potential is odd, $U(-X) = -U(X)$, such solutions strongly localized about $X = 0$ cannot satisfy (6). This allows us to conjecture nonexistence of stable solitons localized about the point $X = 0$ for odd potentials. In particular, in the case of cos-like potential

$$U(X) = 2 \cos(2X), \quad (10)$$

explored below in the present paper: localized modes with a defined symmetry can be excited only in the vicinity of one of the points $X_n = \pi n$ where n is an integer.

Considering solutions localized about $X = 0$ for an even potential $U(X) = U(-X)$ one can identify four types of the modes. They can be classified in terms of the symmetry properties acquired with respect to the periodic potential, considered earlier for a atomic-molecular BEC [7] and for a single-component BEC [13].

The diversity of modes makes it is desirable to establish a convenient terminology for their identification. To this end we classify states according to their symmetry properties with respect to the minima of the periodic potential around which are localized. A classification of this type was introduced in Refs. [7, 13], for atomic-molecular BECs and single-component BECs, respectively, in terms of four single component states. These states are the OS – *on-site symmetric* and OA – *on-site antisymmetric* modes, which are respectively symmetric and antisymmetric with respect to a minimum of the OL, hereafter referred as *lattice site*, and the IS – *inter-site symmetric* and IA – *inter-site anti-symmetric* modes which are respectively symmetric and antisymmetric with respect to a maximum of the OL (the center of the symmetry is the middle point between two lattice sites). Notice that these symmetry properties are the same as for intrinsic localized modes of nonlinear lattices, as one could expect from the tight-binding approximation based on the properties of Wannier functions [14] and reducing the periodic GP equations to discrete lattices [7, 15]. Except for the OS solution, which is always stable, the other types of gap solitons are usually unstable in the one component case [13]. However, from (9) one can expect that gap solitons which have the same symmetry properties

in both components should exist and may be stable. The respective modes will be characterized by a double indexing, like for example OS-OS, OS-OA, etc., the first and second pairs of letters referring to the first and second components, respectively. The modes OS-OS, OA-OA, IS-IS, and IA-IA will be called the "equal-symmetry" two-component modes, while modes OS-OA, IS-IA, etc. will be called mixed symmetry modes, with an evident meaning in the notation.

C. Spinor condensates

Although our results have general character, and can be applied to any binary mixture of BECs, either spinor or of different species, to be specific we focus on spinor BECs. Such condensates are available experimentally. As example we mention mixtures of the hyperfine states $|F = 1, m_F = -1\rangle$ and $|F = 2, m_F = 1\rangle$ as well as of the states $|F = 2, m_F = 1\rangle$ and $|F = 2, m_F = 2\rangle$ of ^{87}Rb atoms produced in [16] and [17], respectively. For a spinor mixture $m_1 = m_2 = m$, $M = m/2$, and the potential (10) the equations (5) are simplified

$$\mu_1 \Phi_1 = -\frac{1}{2} \frac{\partial^2 \Phi_1}{\partial X^2} - V_0 \cos(2X) \Phi_1 + (\chi_1 |\Phi_1|^2 + \chi |\Phi_2|^2) \Phi_1 \quad (11a)$$

$$\mu_2 \Phi_2 = -\frac{1}{2} \frac{\partial^2 \Phi_2}{\partial X^2} - V_0 \cos(2X) \Phi_2 + (\chi |\Phi_1|^2 + \chi_2 |\Phi_2|^2) \Phi_2 \quad (11b)$$

where nonlinear coefficients are given by $\chi_1 = \Omega^{-1} a_{11}/|a_{11}|$, $\chi_2 = \Omega a_{22}/|a_{11}|$, and $\chi = 2a_{12}\Omega/[|a_{11}|(\Omega^2 + 1)]$ with $\Omega = \sqrt{\omega_2/\omega_1}$.

In order to fix parameters we recall that the thermodynamical stability of a homogeneous binary mixture is determined by the condition [18] $\Delta > 0$, where

$$\Delta = \chi_1 \chi_2 - \chi^2. \quad (12)$$

Using this fact as the reference point we will consider the following three situations $\Delta > 0$, $\Delta < 0$ and $\Delta = 0$ (we however emphasize that, generally speaking, these condition should not be considered as the stability/instability conditions for localized modes). Before going into details of numerical simulations, we observe that interchange of the regimes with different Δ can be experimentally achieved either by means of Feshbach resonance affecting scattering lengths a_{ij} or by means of using transverse magnetic trap, i.e. geometry of the trap, resulting in different ω_j for different components, say, in $\Omega = \sqrt{2}$ for the mixtures of hyperfine states $|F = 2, m_F = 1\rangle$ and $|F = 2, m_F = 2\rangle$ of ^{87}Rb atoms in a magnetic trap [17].

III. LOCALIZED MODES OF REPULSIVE BEC MIXTURES WITH UNBALANCED NUMBER OF ATOMS (LIMIT $N_1 \gg N_2$).

A. Defect modes

Let us consider the limit $N_2 \rightarrow 0$. For the first step, neglecting contribution of the second component, $|\Phi_2|^2$, one can solve equation (11a) in the form

$$\mu_1 \Phi_1^{(0)} = -\frac{1}{2} \frac{\partial^2 \Phi_1^{(0)}}{\partial X^2} - V_0 \cos(2X) \Phi_1^{(0)} + \chi_1 |\Phi_1^{(0)}|^2 \Phi_1^{(0)} \quad (13)$$

to find localized modes for a given value of the chemical potential μ_1 . In what follows we focus only on symmetric modes belonging to the lowest branch of the solutions, and therefore referred to as the *fundamental mode*. As the second step, in the same approximation, i.e. neglecting $|\Phi_2|^2$, one can consider (11b) with $|\Phi_1^{(0)}|^2$ found from (13):

$$\mu_2 \Phi_2^{(0)} = -\frac{1}{2} \frac{\partial^2 \Phi_2^{(0)}}{\partial X^2} + V_{eff}(X) \Phi_2^{(0)} \quad (14)$$

where the effective potential is defined as:

$$V_{eff}(X) = -V_0 \cos(2X) + \chi |\Phi_1^{(0)}|^2. \quad (15)$$

After finding discrete eigenvalues μ_2 for a given μ_1 , one can scan the gap for the first component varying μ_1 and obtaining all eigenvalues $\mu_2(\mu_1)$. In Fig. 1 we present the results of this procedure for the cases $\Delta > 0$ and $\Delta < 0$.

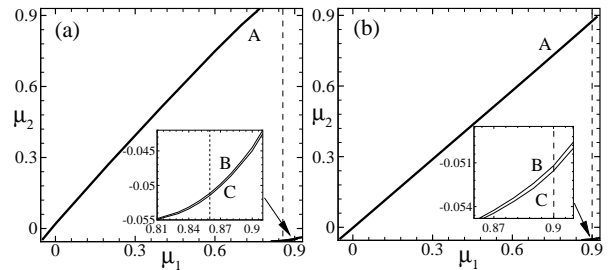


FIG. 1: Discrete levels in the first lowest gaps $\mu_{1,2} \in [-0.055, 0.92]$. The insets show zoom of branches B (OA symmetry) and C (OS symmetry). The amplitude of the OL is $V_0 = 1$. (a) and (b) correspond to different sets of nonlinear coefficients $\chi_1:\chi_2:\chi$ such as in (a) 1:1.584:1.231 ($\Delta > 0$) and in (b) 1:0.942:0.971 ($\Delta < 0$, these relations are taken from [16]). The dashed lines in (a) and (b) correspond to the cross sections at $\mu_1 = 0.86$ and $\mu_1 = 0.9$, respectively.

The physical meaning of the above procedure consists in the approximation of a localized modes Φ_1 , Φ_2 in the limit $N_2 \rightarrow 0$. In this limit, the wavefunction of the second component, Φ_2 , appears as a *defect mode* and, strictly speaking, does not describe the atomic distributions at a finite N_2 . Since however, the solution at $N_2 \approx 0$

is known, departing from it and using an iterative procedure one can construct the solutions for $N_2 > 0$. This approach is based on the following important statement (whose arguments are presented in Appendix A): *If μ_1 and μ_2 as well as V_{01} and V_{02} are fixed, then the localized modes of (5) are isolated.* When $\mu_{1,2}$ varies one can speak about *families* of the nonlinear localized modes.

Before performing the search of localized modes, let us discuss in more details, the results of the above analysis of defect modes. In Fig. 1 three branches of the solutions are shown for different signs of Δ . The branches A correspond to the case where the chemical potentials are approximately equal. In order to understand their occurrence let us consider a solution of Eqs. (11) in the form $\Phi_2 = \alpha\Phi_1$ where α is a constant, which without loss of generality can be considered real. Such a solution exists for $\mu_1 = \mu_2$ and $\alpha^2 = (\chi - \chi_1)/(\chi - \chi_2) > 0$ and below will be referred to as a *trivial solution*. In order to obtain the linear limit (13), (14) one has to consider $\alpha \rightarrow 0$, what is possible only for $\chi_1 = \chi$. In this last case the branches A would coincide with the diagonals of the boxes in Fig. 1. In the cases at hand $\chi_1 \approx \chi$, what explains deviations of the lines A from the diagonals.

The most interesting results, however, are shown in the insets of Fig. 1, where one can observe the two other branches of the solution of the eigenvalue problem (14) – branches B and C. These modes appear in the vicinity of the opposite gap edges for the first and the second components, as this is illustrated in Fig. 2(a) for the case $\Delta > 0$: the eigenvalues are located near the top of the gap for the first component and in the vicinity of the bottom of the gap for the second component. For $N_2 > 0$ (but small) these eigenvalues give rise to OS and OA modes which are characterized by a small difference in energies. Their shapes are shown in Fig 3.

As we have already mentioned these solutions appear as defect modes, what is illustrated in Fig. 2 where we show the fundamental localized mode of the first component near the upper edge of the gap (panel (b)), corresponding potential V_{eff} and the respective energy levels, which can be interpreted as defect modes (panel (c)). The two eigenvalues B and C can be viewed as a splitting of discrete defect level (similar to the level splitting in a double-well potential).

A number of the defect modes depends on the amplitude of the potential V_0 . In all our cases the energy differences between the modes were very small, what makes it convenient to speak about appearance of the pairs of the modes. Then, one can determine V_n , such that for $V_n < V_0 < V_{n+1}$ there exist n pairs of the defect modes (simultaneously with the fundamental mode). In particular, for the cos-like potential and $\Delta > 0$ ($\Delta < 0$) we have found numerically that $V_1 \approx 0.43$, $V_2 \approx 1.42$ ($V_1 \approx 0.61$, $V_2 \approx 2.01$).

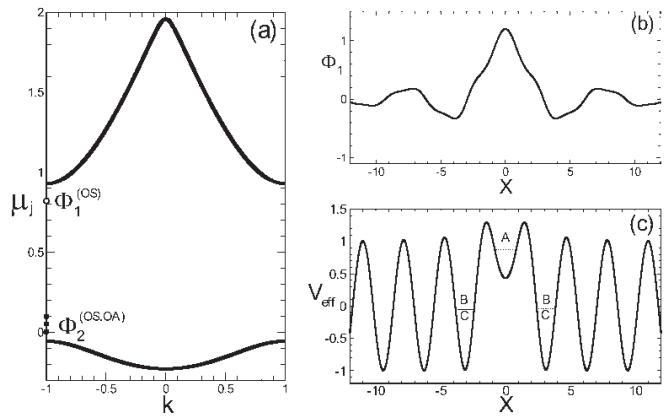


FIG. 2: (a) Band structure and localized levels for the values of parameters fixed as the case $\Delta > 0$ in Fig. 3: the fundamental component at $\mu_1 = 0.86$ (open circle) has OS profile, while the second component (filled circles) is given for both OS and OA profiles considered at the same values of $\mu_2 = 0; 0.05, 0.1$ (see corresponding profiles in Fig. 3). (b) The profile of the fundamental mode, Φ_1 , obtained in the limit $N_2 = 0$. (c) The shape of the respective effective potential (15).

B. The modes with $N_1 \gg N_2$.

We have introduced Eqs. (13), (14) for the sake of approximation of localized modes in the limit $N_2 \ll N_1$. In order to construct the solutions emerging from the branches B and C we use an iterative procedure starting with the solutions obtained for $N_2 \approx 0$. Fig. 3 shows examples of the obtained results.

The mode for the second component bifurcates from the zero-solution. Its amplitude grows with the detuning of the chemical potential μ_2 towards the center of the gap [see Fig. 3(c)-(f) and Fig. 2 (a)], what is accompanied by the increase of the number of particles N_2 .

In Fig. 4 we present the dependence of the number of particles in the second component, N_2 on μ_2 deviating from the corresponding values B and C (see Fig. 1). We notice that in our procedure of search of the modes the profile of the fundamental component also changes with μ_2 . The change, however, is very small, it corresponds to the change of the number of particles in the first component of order of 10^{-3} , and therefore is practically invisible on the scale of Fig. 3(a), (b).

To study dynamical stability of the obtained modes we performed direct numerical integration of equations (4) with $m_1 = m_2$ and $\omega_1 = \omega_2$. As initial conditions we used perturbed stationary solutions obtained using the iterative procedure, the amplitude of perturbation being of the order of 5%.

First, in Fig. 5 we show the case $\Delta > 0$. One can see that the time evolution of the two-component soliton is stable. By switching off the coupling parameter, i.e. setting $\chi = 0$, one obtains the system of two uncoupled GP equations. The dominant fundamental component is close, in some sense, to an OS mode of the single GP

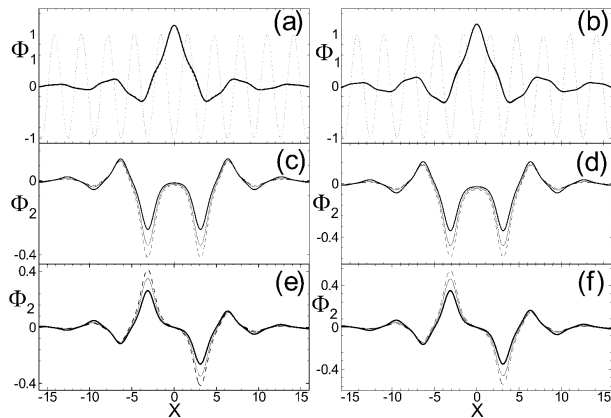


FIG. 3: Localized OS (panels (a)-(d)) and OA (panels (e) and (f)) modes for $\Delta > 0$ (the left column) and for $\Delta < 0$ (the right column) with the same parameters as in Fig. 1. In (a) and (b) the profiles of the first component are shown for $\mu_1 = 0.86$ and $\mu_1 = 0.9$ (indicated by dashed lines in Fig. 1), correspondingly. In [(c),(d)] OS and in [(e),(f)] OA solutions for the second component corresponding to branches C and B from Fig. 1 are shown. Thick, thin, and dashed lines correspond to $\mu_2 = 0.0; 0.05$ and 0.1 , respectively. The dotted line in (a), (b) shows the periodic potential (thin and dashed lines in (a) and (b) are not distinguishable on the scale of the figure).

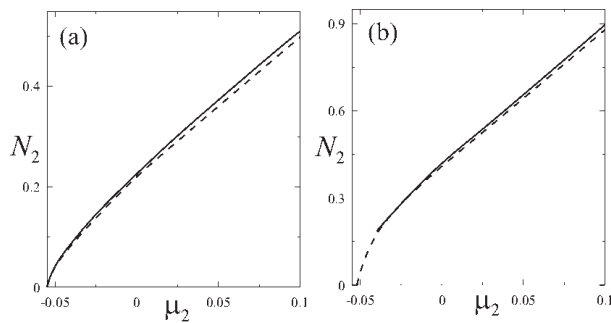


FIG. 4: The number of particles of the second component *vs* μ_2 for the cases $\Delta > 0$ (panel a) and $\Delta < 0$ (panel b) corresponding to Fig. 3. In (a) $\mu_1 = 0.86$ with $N_1 \approx 3.17$ and in (b) $\mu_1 = 0.9$ with $N_1 \approx 3.42$. Here solid and dashed lines correspond to second component with OS and OA symmetry.

equation with the periodic potential and that is why it is stable. The second component, representing two in-phase humps and originally coupled by the effective potential due to the first component, becomes unstable at $\chi = 0$. The two humps in the absence of first component, which the played role of the effective barrier between them, start to move towards each other and overlap. However due to the large velocity after collision two wave packets start to move outwards the center. The described behavior is observed at the initial stages of the evolution shown in Fig. 6 (a), (b). At latter times, reaching the turning point they change the direction of motion towards the center. After several periods of damped oscillations the one-hump OS mode is created. The out-of-phase distri-

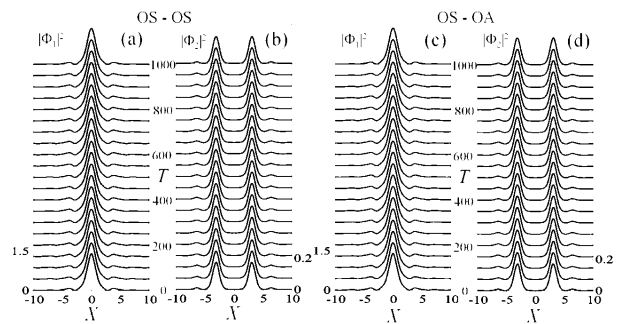


FIG. 5: Dynamics of density of the first component in (a), (c) and of the second component in (b), (d). In [(a), (b)] and [(c), (d)] initial profiles are taken from Fig. 3 [(a), (c)] and [(a), (e)], correspondingly, with $\mu_1 = 0.86$ and $\mu_2 = 0.1$.

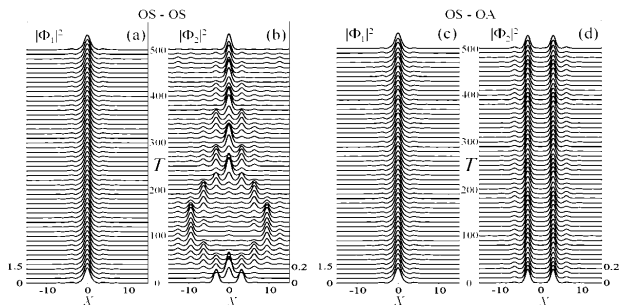


FIG. 6: The same initial conditions as in Fig. 5 with $\chi = 0$. The real domain of calculation is $[-14\pi; 14\pi]$.

bution of the second component, shown in Fig. 6 (d) is stable representing a single-component stable OA mode.

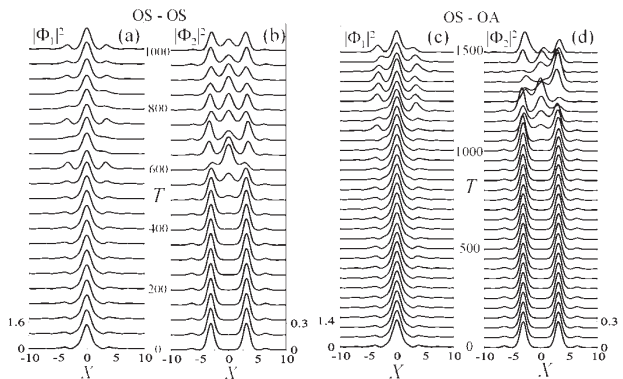


FIG. 7: The dynamics of density profiles in (a), (c) of the first component with OS symmetry and in (b), (d) of the second component with OS and OA symmetries. Initial distributions are as in Fig. 3 [(b),(d)] and [(b),(f)] with $\mu_1 = 0.9$ and $\mu_2 = 0.1$, respectively.

Next we investigated the case $\Delta < 0$. Typical results are shown in Fig. 7, where one observes instability of the both OS-OS (panels (a) and (b)) and OS-OA (panels (c) and (d)) modes. It has been checked that the time at which the instability is developed increases when μ_2

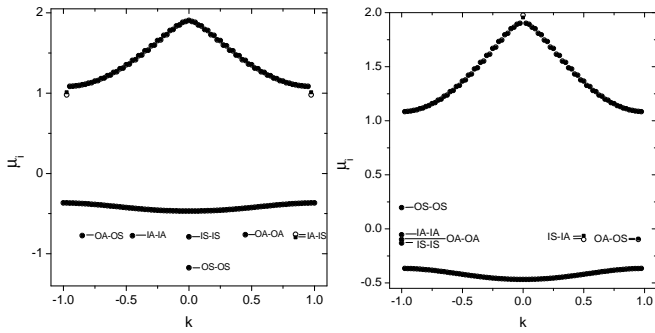


FIG. 8: Band structure and bound state levels of the two component BEC in OL with all attractive $\chi_{11} = \chi_{22} = \chi_{12} = -0.5$, (left panel) and all repulsive $\chi_{11} = \chi_{22} = \chi_{12} = 0.5$, (right panel) interactions. For both cases the amplitude of the OL is $V_0 = 1.5$ and the number of atoms is $N_1 = 1.5, N_2 = 0.98$. Open circles refer to the first component while filled squares refer to the second component. Notice that all equal symmetry modes are degenerated. Also notice the presence of a bound state near the edge of the upper band (left panel) and a bound state in the second gap (right panel).

approaches the lowest edge of the gap, tending to infinity as μ_2 approaches $\mu_{B,C}$ and respectively as $N_2 \rightarrow 0$.

IV. LOCALIZED MODES WITH BALANCED NUMBER OF ATOMS (LIMIT $N_1 \simeq N_2$).

Let us now turn to the study of two-component localized modes with a *balanced* i.e. with the same or with similar number of particles in each component. These modes can be of equal symmetry or of mixed symmetry type. Some of the equal symmetry modes were also found in Ref. [5]. Balanced mixed symmetry modes have not been discussed before. In contrast to the equal symmetry solutions, which for many aspects are similar to standard modes of the single component GPE, the mixed state symmetries are more specific for multicomponent BEC systems in OL displaying interesting stability properties.

Thus, while the OA and the OA-OA modes are unstable for the one- and two-component system, respectively, the coupling of the OA mode with an OS mode gives rise to a stable OS-OA mixed state of two-component BEC in OL. The same situation occurs with the IS and IA modes. In the following we show that these mixed symmetry solutions exist for both attractive and repulsive inter and intra specie interactions and together with the on site OS-OS solution, they represent stable localized excitation of a two-component BEC in OL.

In Fig. 8 we depict the lowest part of the band structure of Eqs. (11) obtained for the cases of all attractive $\chi_{11} < 0, \chi_{22} < 0, \chi < 0$ (left panel) and all repulsive $\chi_{11} > 0, \chi_{22} > 0, \chi > 0$ (right panel) interactions. We see that the nonlinearity induces in both cases a number of bound states in the band gap structure, located in the forbidden zone below the first band for the attractive case

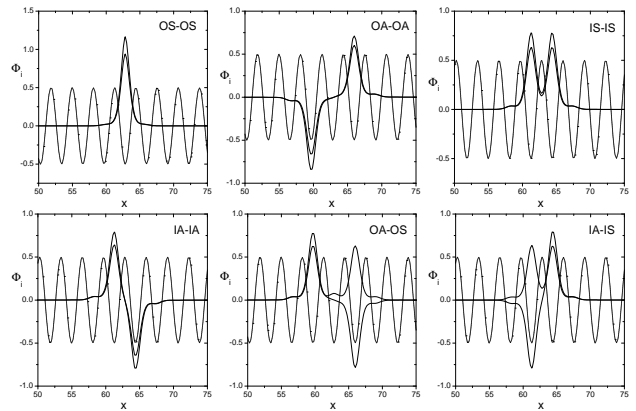


FIG. 9: Condensate wavefunctions of two-component BEC in OL corresponding to the bound state levels in the left panel of Fig. 8 (all attractive case). Thick and thin lines refer to first and second component, respectively (open circles and filled squares in Fig. 8). To identify the symmetry of the solutions, lattice potentials (scaled by a factor 3) have been shown by thin dotted line.

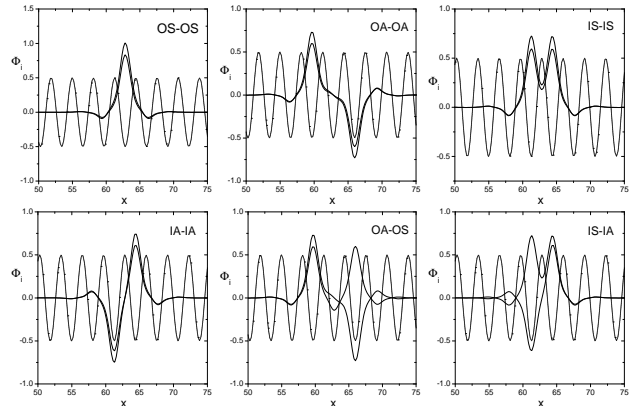


FIG. 10: Condensate wavefunctions of two-component BEC in OL corresponding to the bound state levels in the right panel of Fig. 8 (all repulsive case). Thick and thin lines refer to first and second component, respectively (open circles and filled squares in Fig. 8). To identify the symmetry of the solutions, lattice potentials (scaled by a factor 3) have been shown by thin dotted lines.

or in the gap between the first two bands for the repulsive case. Similar bound states can also form inside the upper band gaps (see right panel of Fig. 8). In this figure bound state levels are labeled by symmetry type symbols close to the pair of the corresponding levels. Thus the OS-OS symbol denotes a bound state consisting of an OS state in both components with the corresponding chemical potentials labeled by the open circle and the full square close to the symbol. We find that the two component bound states of same symmetry type are degenerate in energy (chemical potential) both for all attractive and all repulsive interactions. In contrast to the states OS-OS and OA-OA which are found to be stable also in absence of the interspecies interaction ($\chi = 0$), the states IA-IA

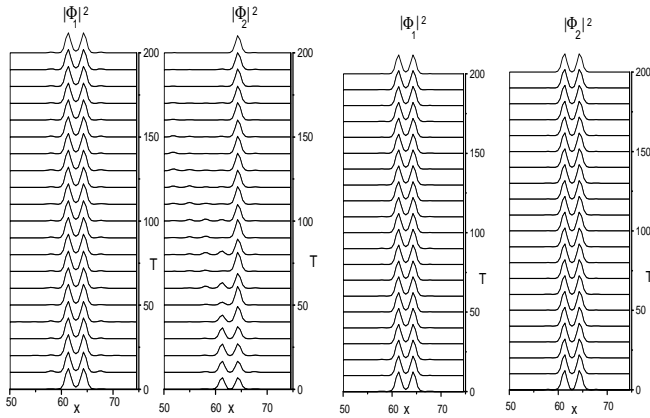


FIG. 11: Time evolution of the density profiles of the IS-IA mode of the all attractive case in Fig. 9, in absence ($\chi = 0$, left panels) and in presence ($\chi = -0.5$, right panels) of interaction between the two components.

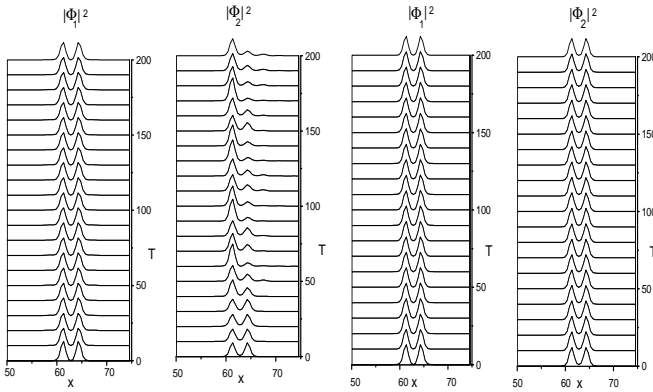


FIG. 12: The same as in Fig. 11 but for the IS-IA mode of the all repulsive case in Fig. 10.

is stable only in presence of interaction between the two species and the state IS-IS is unstable also in presence of the interspecies interaction (in this case the state decays a bit faster without interaction). In Figs. 9 and 10 we depict the eigenstates corresponding to the bound states shown in Fig. 8.

In addition to the equal symmetry two-component bound states there are also states with mixed symmetry such as the OA-OS and the IS-IA bound states. These states are very stable and represent new excitations of the two-component system since they can exist only in presence of the interspecies interaction. In particular we find that the mixed symmetry states OA-OS and IA-IS exist and are stable under time evolution only due to the interspecies interaction. This is shown in Figs. 11 and 12 for the IS-IA mode of the attractive and repulsive cases in Fig. 9 and Fig. 10, respectively. We see that in both cases modes are stable in both components only in presence of interaction and the switching off of the interaction makes the second component to decay into an OS mode

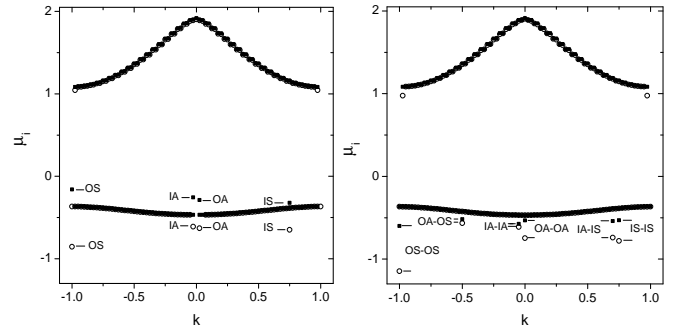


FIG. 13: Band structure and bound state levels of the two component BEC in OL with intra and inter species interactions fixed as $\chi_1 = -0.5, \chi_2 = 0.5, \chi = 0$ (left panel) and as $\chi_1 = -0.5, \chi_2 = 0.5, \chi = -0.5$ (right panel). Other parameters are $V_0 = 1.5, N_1 = 1.5, N_2 = .98$. Open circles refer to the first component, filled squares to the second one. Notice that in this case the equal symmetry modes are non degenerated. Also notice the presence of localized modes near the edge of the upper bands.

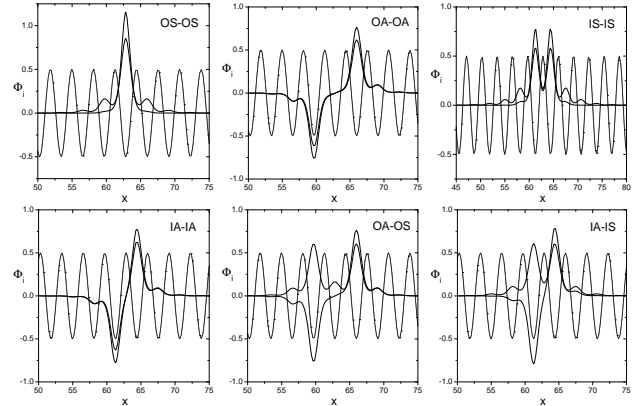


FIG. 14: Condensate wavefunctions of two-component BEC in OL corresponding to the bound state levels in the right panel of Fig. 13. Thick and thin lines refer to first and second component, respectively (open circles and filled squares in Fig. 13). To identify the symmetry of the solutions, lattice potentials (scaled by a factor 3) have been shown by thin dotted lines.

with emission of matter.

We have also investigated the case of mixed interactions $\chi_1 < 0, \chi_2 > 0, \chi < 0$ (see Figs. 13,14). In contrast with previous cases where bound state levels were located in the semi-infinite gap or in the first band gap,

in the case of mixed interactions the bound states are all below the first band, in spite of the fact that the second component has a repulsive character. In absence of the interaction, however, the bound states of the second component are indeed located in the first band gap as expected (see left panel of Fig. 13). By increasing the strength of the interspecies interaction these eigenvalues get shifted below the first band, this being a consequence of the attraction between the two components (for repulsive interspecies interactions the levels would be repelled into the gap making the formation of bound states more difficult). Also notice that in contrast with the all attractive and all repulsive cases, the equal symmetry localized modes (as well as the mixed symmetry ones) are non degenerate (the components of the bound state have different chemical potentials), this being due to the fact that the unperturbed levels belong to different band gaps. By changing the values of χ (by means of Feshbach resonances) one can indeed change the position of the bound state levels with respect to the band structure, this affecting the properties (in particular the stability) of the corresponding localized state. Similarly properties are found also for other parameter choices and for two-component modes states of higher band gaps.

V. BREATHERS.

The method of construction of localized modes based on continuation from the limit $N_2 \approx 0$, can be used for obtaining rather different solutions of the coupled GP equations with a periodic potential, when all the nonlinearity coefficients are equal $\chi = \chi_1 = \chi_2$. Indeed, in that case the system (5) takes the form

$$i \frac{\partial \Phi_j}{\partial T} = -\frac{1}{2} \frac{\partial^2 \Phi_j}{\partial X^2} - V_0 \cos(2X) \Phi_j + \chi (|\Phi_{1j}|^2 + |\Phi_{3-j}|^2) \Phi_j \quad (16)$$

and is invariant under transformation

$$\varphi_1 = (\Phi_1 + \Phi_2)/\sqrt{2}, \quad \varphi_2 = (\Phi_1 - \Phi_2)/\sqrt{2}. \quad (17)$$

Let us now assume that one of the component, Φ_j , is much larger than the other one, say $N_1 \gg N_2$. By using the method described in the previous section we can find stationary solutions of the coupled GP equations in the form $\Phi_j(X, T) = \Phi_j(X) e^{-i\mu_j T}$ (notice that the chemical potential of the large-amplitude component is located near the top of the gap while that of the small-amplitude component is near the bottom of the gap, such that $\mu_1 - \mu_2$ is of the order of the energy gap. Thus, substituting the stationary solutions $\Phi_j(X, T)$ into (17) we readily obtain new solutions $\varphi_j(X, T)$ characterized by the amplitudes of the same order and by *two* chemical potentials, i.e. representing breathers (in the sense of the periodically oscillating density of the condensate).

In Fig. 15 we show the dynamics of such breathing solution which appears to be dynamically stable.

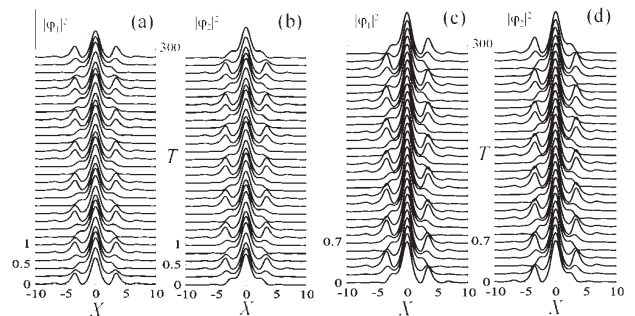


FIG. 15: In [(a),(c)], [(b),(d)] dynamics of the density of the $|\varphi_1|^2$ and $|\varphi_2|^2$ are shown correspondingly. Initial profiles for Φ_j are calculated for the parameters $\chi = 1$, $V_0 = 1$, $\mu_1 = 0.88$ and $\mu_2 = 0.1$. In [(a), (b)] the OS and [(c), (d)] the OA profile of Φ_2 was used.

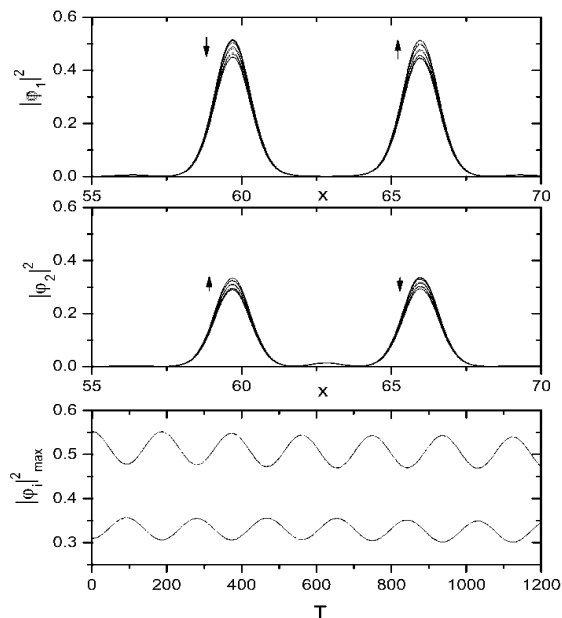


FIG. 16: Gap-breather mode of OA-OS type for the case $\chi_1 = \chi_2 = \chi = 0.5$, $V_0 = 1.5$, and for number of atoms $N_1 = 1.5$, $N_2 = 0.98$. The top panels show ten snapshots of the density profiles of the first (first panel) and second (second panel) component of the gap-breather taken at regular intervals of time during one period $T = 187.86$ of oscillation. The bottom panel show the amplitude of the left peaks of both components as a function of time. The arrows indicate that the oscillation of the two components occurs in opposite phase.

Besides two-components breather modes with unbalanced number of atoms, we also find breather modes with mixed symmetry which are very stable even for relatively large values of the number of atoms in both components. The existence of these modes is expected both from previous considerations and from the existence and stability of the mixed symmetry modes with balanced number of atoms discussed in the previous section.

In Fig. 16 a gap-breather mode of the OA-OS type is depicted for the case of all repulsive interactions. We see that the oscillations of the two components are out of phase and are very regular, persisting for very long time without any emission of matter, this indicating that the mode is indeed very close to an exact breather solution of the two-component GPE system.

VI. CONCLUSIONS

In the present paper we have presented a variety of localized modes, having stationary localized density distribution, and breathers, characterized by periodically varying density, in binary mixtures of Bose-Einstein condensates. In particular, we have considered modes having either close or very different numbers of atoms (we termed them balanced and unbalanced modes) and characterized by the same or different symmetries of the atomic distributions in each components. We have suggested algorithms of systematic finding families of the modes. We exploited the fact that unbalanced modes bifurcate from the linear defect modes, the defect being understood as a localized excitation of one of the components in the absence of another component. This allowed us construct exact breather modes in a systematic way.

We have introduced the classification of the modes on the basis of four possible distributions of each of the components, what in the general case results in the modes of 8 different types, which can be designated as BC₁-BC₂, where B stands either for "O" in the case of the distribution centered in a local minimum of the periodic potential or for "I" in the case of the mode centered in the maximum of the potential, and C_j stands for S or A depending whether the wavefunction of the the *j*-th component is even (S) or odd (A).

Although our analysis was concentrated on spinor condensates, it allows for straightforward generalization for arbitrary two-component system described by coupled nonlinear Schrödinger equations with periodic coefficients.

Acknowledgments

HAC acknowledges support of the FCT thorough the grant SFRH/BD/23283/2005. VAB was supported by

the FCT grant SFRH/BPD/5632/2001. VVK acknowledges support from Ministerio de Educación y Ciencia (MEC, Spain) under the grant SAB2005-0195. M. S. acknowledges partial financial support from the MIUR, through the inter-university project PRIN-2005, and from the (CNISM) Consorzio Nazionale Interuniversitario per le Scienze Fisiche della Materia. The work of HAC, VAB, VVK, and GLA was supported by the FCT and FEDER under the grant POCI/FIS/56237/2004.

APPENDIX A: SOME COMMENTS ON THE SHOOTING METHOD

In this Appendix we briefly outline the implementation of the shooting method for finding localized solutions of (5). Let $\mu_{1,2}$ and V_{01}, V_{02} be fixed and μ_i belong to gaps of the potentials $V_{0i}U(X)$. In the limit $X \rightarrow \infty$ the equations in (5) separate. Both of them become linear Hill equations and the asymptotics of $\Phi_{1,2}(X)$ as $X \rightarrow \infty$ are given by the formula ($j = 1, 2$)

$$\Phi_j(X) \sim C_j e^{-\gamma_j X} H_j(X), \quad (\text{A1})$$

where 2π -periodic functions $H_{1,2}$ and values $\gamma_{1,2} > 0$ are uniquely defined by the parameters of equations. The parameters $C_{1,2}$ specify the solutions of (5) which tend to zero at $X \rightarrow \infty$. If $C_{1,2}$ are fixed the solution $\Phi_{1,2}(X; C_1, C_2)$, subject to the conditions (A1) at $X \rightarrow \infty$, can be found by shooting backward starting from large enough value of X where this asymptotics is valid. Let us consider, for the sake of definiteness, *even* localized solutions of (5). They have to satisfy the conditions

$$\frac{d\Phi_1(0; C_1, C_2)}{dX} = 0; \quad \frac{d\Phi_2(0; C_1, C_2)}{dX} = 0. \quad (\text{A2})$$

This is the system of two equations for two variables C_1 and C_2 . Generically, the solutions of this system are *isolated* [in the sense that if C_1^0 and C_2^0 is a solution there is some neighborhood of $(C_1^0; C_2^0)$ which does not contain other solutions of (5)]. Similar arguments hold for odd and also for non-symmetric solutions of (5). In this way one arrives at the conclusion formulated in the text.

-
- [1] V.A. Brazhnyi and V.V. Konotop, Mod. Phys. Lett. B **18**, 627 (2004).
 - [2] O. Morsch and M. Oberthaler, Rev. Mod. Phys. **78**, 179 (2006).
 - [3] B. Eiermann, *et al.*, Phys. Rev. Lett. **92**, 230401 (2004).
 - [4] N.A. Kostov, *et al.*, Phys. Rev. E **70**, 056617 (2004); K. Kasamatsu and M. Tsubota, Phys. Rev. A **74**, 013617 (2006).
 - [5] E.A. Ostrovskaya and Yu.S. Kivshar, Phys. Rev. Lett. **92**, 180405 (2004).
 - [6] A. Gubeskys, B.A. Malomed and I.M. Merhasin, Phys. Rev. A **73**, 023607 (2006).
 - [7] F.Kh. Abdullaev and V.V. Konotop, Phys. Rev. A **68**, 013605 (2003).
 - [8] Mario Salerno, Phys. Rev. A **72**, 063602 (2005).
 - [9] Yu.V. Bludov and V.V. Konotop, Phys. Rev. A **74**,

- 043616 (2006).
- [10] Beata J. Dabrowska-Wüster *et al.*, Phys. Rev. A **75**, (2007) (in press).
- [11] L. Pitaevskii and S. Stringari, *Bose-Einstein Condensation* (Clarendon Press, Oxford, 2003).
- [12] G.L. Alfimov, V.V. Konotop, and M. Salerno, Europhys. Lett. **58**, 7 (2002).
- [13] M. Salerno, Laser Physics **15**, 620-625 (2005).
- [14] W. Kohn, Phys. Rev. **115**, 809 (1959)
- [15] G. L. Alfimov, P. G. Kevrekidis, V. V. Konotop, and M. Salerno Phys. Rev E. **66**, 046608 (2002).
- [16] C.J. Myatt, *et al.*, Phys. Rev. Lett. **78**, 586 (1997); D.S. Hall, *et al.*, Phys. Rev. Lett. **81**, 1539 (1998); D.S. Hall, *et al.*, *ibid.* **81**, 1543 (1998); M.R. Matthews *et al.*, Phys. Rev. Lett. **81**, 243 (1998); J. Stenger, *et al.*, Nature (London) **396** 345 (1998); H.-J. Miesner, *et al.*, Phys. Rev. Lett. **82**, 2228 (1999); G. Modugno, *et al.*, Science **294**, 1320 (2001); M.R. Matthews, *et al.*, Phys. Rev. Lett. **83**, 3358 (1999); M.R. Matthews, *et al.*, Phys. Rev. Lett. **83**, 2498 (1999); J. Williams, *et al.*, Phys. Rev. A. **59**, R31 (1999).
- [17] P. Maddaloni, *et al.*, Phys. Rev. Lett. **85**, 2413 (2000).
- [18] C.J. Pethick and H. Smith, *Bose-Einstein condensation in dilute gases* (Cambridge, University Press, 2001).

